

ISSN: 0256-307X

中国物理快报

Chinese Physics Letters

Volume 38 Number 3 March 2021

A Series Journal of the Chinese Physical Society
Distributed by IOP Publishing

Online: <http://iopscience.iop.org/0256-307X>
<http://cpl.iphy.ac.cn>

CHINESE PHYSICAL SOCIETY
IOP Publishing

JUST FOR AUTHORS
— CHINESE PHYSICS LETTERS

Ehrenfest Time at the Transition from Integrable Motion to Chaotic Motion

Chuan Zhao(赵川)¹ and Biao Wu(吴飙)^{1,2,3*}¹International Center for Quantum Materials, School of Physics, Peking University, Beijing 100871, China²Wilczek Quantum Center, School of Physics and Astronomy, Shanghai Jiao Tong University, Shanghai 200240, China³Collaborative Innovation Center of Quantum Matter, Beijing 100871, China

(Received 20 November 2020; accepted 7 January 2021; published online 2 March 2021)

Ehrenfest time depends differently on the Planck constant in integrable motion and chaotic motion. We study how its dependence on the Planck constant changes when there is a continuous transition from regular motion to chaotic motion. We find that the dependence is a weighted compromise between its two distinct dependences in regular and chaotic motions. The study is carried out with the system of periodically driven anharmonic oscillator. As the system is quite typical, the result may apply generally.

DOI: 10.1088/0256-307X/38/3/030502

When a well-localized wave packet of a single particle moves in a smoothly varying potential, the center of the wave packet will follow the classical dynamics for a period of time. This time scale is called Ehrenfest time.^[1] Ehrenfest time has been studied extensively and systematically.^[2–11] It is found that for the integrable system (or motion) Ehrenfest time is inversely proportional to the square root of the Planck constant \hbar ^[12–14] and for the chaotic system (or motion) Ehrenfest time is proportional to $\ln \hbar^{-1}$.^[5–7,15] According to the KAM theorem,^[16] the transition from regular motion to chaotic motion in classical dynamics is gradual. Therefore, it is interesting to know how the dependence of Ehrenfest time on the Planck constant changes at the transition from integrable motion to chaotic motion.

We study how Ehrenfest time changes its dependence on the Planck constant when regular motion gradually switches to chaotic motion. We find that at this kind of transition the Ehrenfest time is a mixture of that of integrable dynamics and chaotic dynamics. This mixture is determined by how much the initial wave packet occupies an integrable region and how much it occupies in a chaotic region. Our study is carried out with a one-dimensional, periodically driven anharmonic oscillator, but the methods and conclusions can be easily applied to other models with chaotic dynamics.

Anharmonic Oscillator with Periodic Driving. In this work, we focus on a one-dimensional anharmonic oscillator with periodic driving. By varying the system parameters, in particular, the driving strength, we can change the system's dynamical behavior from integrable to chaotic. The system Hamiltonian is

$$H = \frac{p^2}{2m_0} + \frac{1}{2}m_0\omega_0^2x^2 + Dx^4 + Ax \sin(\omega t), \quad (1)$$

where m_0 is the mass of the particle, t is the time, and ω_0 is the frequency of the system without driving and anharmonicity. Our Hamiltonian is similar to the one used in Ref. [15], but the coefficient D of the quadratic term here is positive so that its potential is not a double-well. Without the driving item ($A = 0$), the system is totally integrable and has been studied in Ref. [14]. With appropriate parameters, the system has both chaotic and integrable dynamics, and the relative proportion of chaotic regions and integrable regions in the phase space can be adjusted by parameters such as driving strength A and driving frequency ω . To numerically investigate the quantum and classical dynamics of this system, we set the Planck constant in the Schrödinger equation as $\hbar = \tilde{\hbar}\hbar_0$, where \hbar_0 is the usual Planck constant and the dimensionless constant $\tilde{\hbar}$ can be varied to study the semi-classical limit. For the convenience of numerical calculation, we make all the parameters dimensionless in this manuscript. We use $\sqrt{\hbar_0}/(m_0\omega_0)$ as the unit of length, $\sqrt{\hbar_0 m_0 \omega_0}$ as the unit of momentum, $\hbar_0\omega_0$ as the unit of energy, and $1/\omega_0$ as the unit of time. All of our numerical results in the manuscript are carried out in this dimensionless system. Without loss of generality, we choose the following set of parameters: $\hbar_0 = 1$, $m_0 = 1$, $\omega_0 = 1$, $\omega = 2.1$, $D = 1.8$, $A = 0.5$, for which the classical phase space has both chaotic and integrable regions (see Fig. 1).

A typical classical Poincaré section of our anharmonic oscillator is shown in Fig. 1. It contains mainly four regions. There are one chaotic region E , and three integrable regions F , G , K . Chaotic region E is between two integrable regions F and K .

In our following study, we will examine three different dynamics, single particle classical dynamics, classical ensemble dynamics, and quantum wave packet

Supported by the National Key R&D Program of China (Grants Nos. 2017YFA0303302 and 2018YFA0305602), the National Natural Science Foundation of China (Grant No. 11921005), and the Shanghai Municipal Science and Technology Major Project (Grant No. 2019SHZDZX01).

*Corresponding author. Email: wubiao@pku.edu.cn

© 2021 Chinese Physical Society and IOP Publishing Ltd

dynamics, and compare them to extract Ehrenfest time and quantum time. For a single particle classical initial condition (x_0, p_0) , we construct the following Gaussian wave packet as the initial state for the quantum dynamics,

$$\psi(x) = \frac{1}{(2\pi\sigma_x^2)^{1/4}} \exp \left\{ -\frac{(x-x_0)^2}{4\sigma_x^2} + \frac{ip_0(x-x_0)}{\hbar} \right\}, \quad (2)$$

where σ_x is the width of the initial wave packet. We use the Wigner function of the above Gaussian wave packet as the initial distribution for a classical ensemble dynamics,

$$\rho_c(x, p) = \frac{1}{\pi\hbar} \exp \left\{ -\frac{(x-x_0)^2}{2\sigma_x^2} - \frac{(p-p_0)^2}{2\sigma_p^2} \right\}, \quad (3)$$

where σ_x and σ_p are the widths of the initial classical ensemble in phase space.

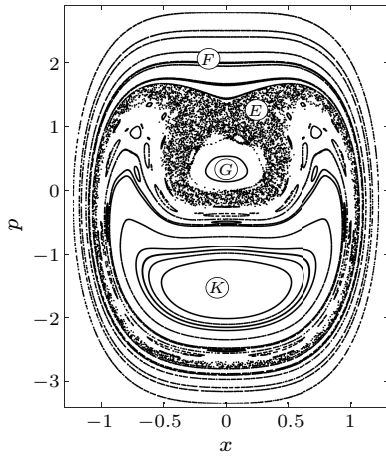


Fig. 1. Classical Poincaré section of our anharmonic oscillator with periodic driving. It is divided into four regions labeled by E, F, G, K .

We are interested in the position of the classical particle $[x_c(t)]$, the averaged position of the classical ensemble that contains 10^5 particles $[\bar{x}_e(t)]$, and the expectation value of x of corresponding quantum wave packet $[\langle x_q(t) \rangle]$. One example is shown in Fig. 2. We find that the expectation value $\bar{x}_e(t)$ matches with the single particle position $x_c(t)$ for a short period and then start to diverge. In contrast, the classical ensemble expectation value $\bar{x}_e(t)$ matches with the quantum wave packet $\langle x_q(t) \rangle$ for much longer time as shown in Figs. 2(a) and 2(b). The shorter time is Ehrenfest time, beyond which the correspondence of a classical particle and the quantum wave packet breaks down as the potential function varies dramatically within the wave packet range. The longer time is the quantum time, beyond which the correspondence between quantum dynamics and classical ensemble dynamics breaks down and quantum phenomena appear, such as quantum tunneling, quantum revival, dynamical localization.^[14,17–20] The dynamics beyond quantum

time in this model is quite complicated and will be addressed in a future publication. In this work we focus on Ehrenfest time.

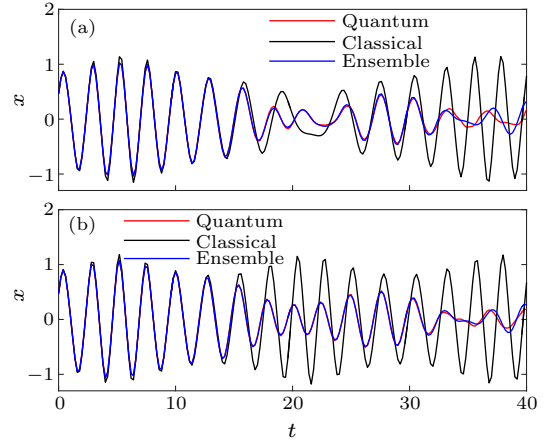


Fig. 2. (a) The time evolutions of a classical particle $x_c(t)$, its corresponding classical ensemble average $\bar{x}_e(t)$, and the corresponding quantum expectation value $\langle x_q(t) \rangle$ in integrable region F under the initial condition $x_0 = 0.46$ and $p_0 = 1.62$; $\hbar = 0.02$. (b) The time evolutions of a classical particle $x_c(t)$, its corresponding classical ensemble average $\bar{x}_e(t)$, and the corresponding quantum expectation value $\langle x_q(t) \rangle$ in chaotic region E under the initial condition $x_0 = 0.47$, $p_0 = 1.74$, $\hbar = 0.02$.

Ehrenfest Times for Integrable Motion and Chaotic Motion. Ehrenfest time has been studied extensively.^[2–11] It is now well known that for the integrable systems Ehrenfest time is inversely proportional to the square root of \hbar ^[12–14] and for the chaotic model Ehrenfest time is proportional to $\ln \hbar^{-1}$.^[5–7,15] Our model allows us to study Ehrenfest time for both integrable case and chaotic case within one system as its Poincaré section contains both integrable region and chaotic region. More importantly, it allows us to study how Ehrenfest time depends on the Planck constant at the transition from integrable motion to chaotic motion.

We first study Ehrenfest time for integrable motion and chaotic motion. For this purpose, we pick one initial condition in the integrable region of the Poincaré section and the other initial condition in the chaotic region. To extract Ehrenfest time from numerical results, we plot the relative difference r between extreme values of $x_c(t)$ and $\bar{x}_e(t)$, which is defined as $r \equiv \frac{|x_c - \bar{x}_e|}{x_c}$, as a function of time as shown in Fig. 3. These evolution curves fit with an exponential function $r = c(e^{\gamma t} - 1)$ after neglecting some big-error points caused by small denominators and mismatches between extreme values of $x_c(t)$ and $\bar{x}_e(t)$. Here c is a constant and we take $c = 10^{-4}$ in this function. The Ehrenfest time is obtained as $\tau_e = 1/\gamma$. The relation between Ehrenfest time and reciprocal of \hbar is illustrated in Fig. 4. For the integrable motion, the Ehrenfest time is $\tau_e \propto \hbar^{-1/2}$; for the chaotic motion, the Ehrenfest time is logarithmic, $\tau_e \propto \ln \hbar^{-1}$. These results are consistent with previous works.^[4,7,10,12–14]

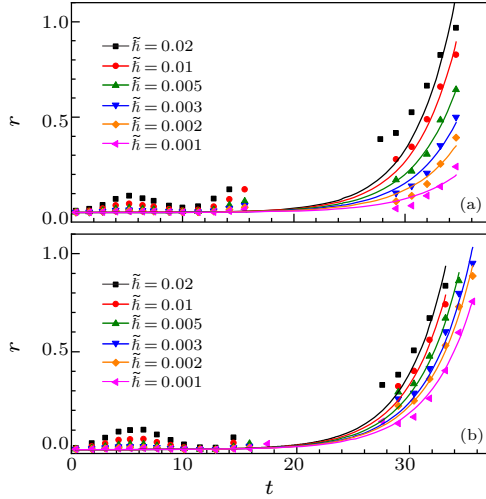


Fig. 3. The relative difference r between the classical position $x_c(t)$ and its corresponding ensemble expectation $\bar{x}_e(t)$ as a function of time for different Planck constants $\tilde{\hbar}$: (a) integrable motions ($x_0 = 0.46$, $p_0 = 1.62$), (b) chaotic motions ($x_0 = 0.47$, $p_0 = 1.74$). Results are fitted by the function $r = 10^{-4}(e^{\gamma t} - 1)$, as indicated by solid lines.

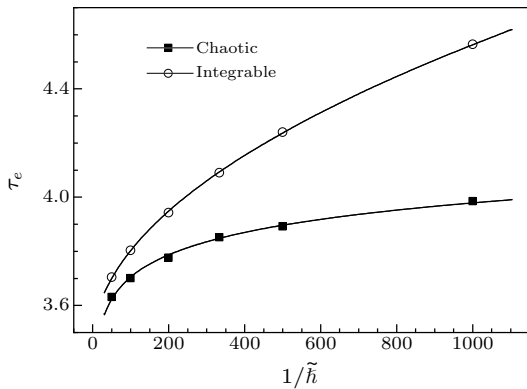


Fig. 4. Relationships between Ehrenfest time τ_e and $1/\tilde{\hbar}$. Integrable Ehrenfest time is fitted by $\tau_e = 0.0352\tilde{\hbar}^{-1/2} + 3.45$, ($x_0 = 0.46$, $p_0 = 1.62$). Chaotic Ehrenfest time is fitted by $\tau_e = 0.119 \ln \tilde{\hbar}^{-1} + 3.16$ ($x_0 = 0.47$, $p_0 = 1.74$).

Transition from Integrable to Chaotic Motion. Although there are only integrable and chaotic motions for classical single particles, there is another motion in addition to integrable and chaotic motion for quantum wave packets. That is the evolution of a wave packet in a region of transition from integrable to chaotic. From previous results, we know that Ehrenfest time for chaotic system is logarithmic, $\tau_e \propto \ln \tilde{\hbar}^{-1}$, distinct from that of integrable system, which is $\tau_e \propto \tilde{\hbar}^{-1/2}$. It is interesting to know how Ehrenfest time depends on the Planck constant at the transition from integrable to chaotic motion.

We pick two points A and B near the boundary of integrable and chaotic regions in the Poincaré section [see Fig. 5(a)]. A is in the integrable region and B is in the chaotic region. We then numerically calculate Ehrenfest time of the wave packets initially centered around these two points A and B for different Planck constants $\tilde{\hbar}$. When $\tilde{\hbar}$ is small, these two wave pack-

ets are separated by the boundary of integrable and chaotic regions. As $\tilde{\hbar}$ becomes larger, the two wave packets partially overlap in the phase space as shown in Fig. 5(a). The relationship between Ehrenfest time and $\tilde{\hbar}$ is plotted in Fig. 5(b), where numerical results are represented by hollow and solid dots with hollow for A and solid for B . The curves represent the fitting of the chaotic and integrable systems using the first four data with largest $\tilde{\hbar}^{-1/2}$. The numerical data for small $\tilde{\hbar}^{-1/2}$ are found between the two curves.

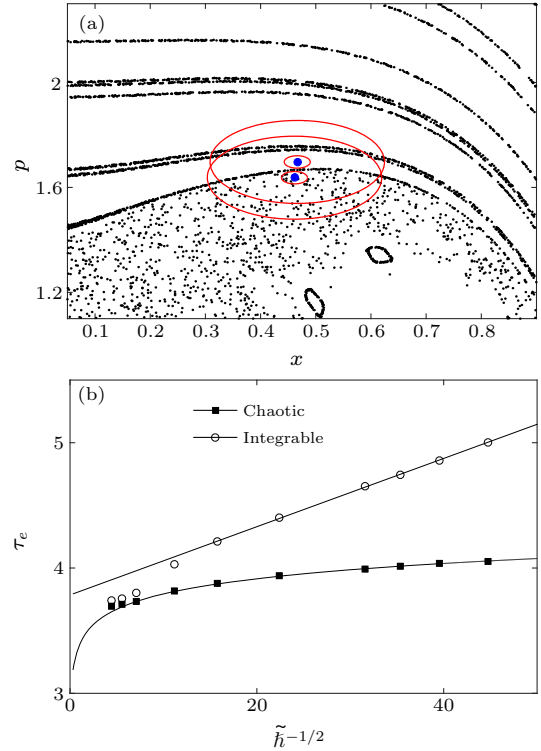


Fig. 5. (a) Two points A ($x_0 = 0.4664$, $p_0 = 1.697$) and B ($x_0 = 0.4614$, $p_0 = 1.637$), separated by the boundary of integrable-chaotic regions in the Poincaré section. They are indicated with blue solid dots. There are two red circles around each point: the small one indicates the size of wave packets with $\tilde{\hbar} = 0.001$, and the large one indicates the size of wave packet with $\tilde{\hbar} = 0.05$. (b) Ehrenfest time as a function of $\tilde{\hbar}^{-1/2}$. Numerical results are shown by hollow and solid dots. Four hollow or solid dots with largest $\tilde{\hbar}^{-1/2}$ are used for fitting each curve. Ehrenfest time of integrable motion is fitted by the function $\tau_e = 0.0272\tilde{\hbar}^{-1/2} + 3.78$, and Ehrenfest time of chaotic dynamics is fitted by the function $\tau_e = 0.0879 \ln \tilde{\hbar}^{-1} + 3.39$.

The above numerical results are not hard to explain. When $\tilde{\hbar}^{-1/2}$ is large ($\tilde{\hbar}$ is small), the wave packets are well localized in either the integrable region or chaotic region. It means that the wave packet dynamics is either integrable or chaotic. When $\tilde{\hbar}^{-1/2}$ is small ($\tilde{\hbar}$ is large), the wave packets become wider, overlapping with both integrable and chaotic regions. In this case, the wave packet consists of two parts: one part propagates largely according to the integrable dynamics and the other part largely propagates according to the chaotic dynamics. The overall result is a mixture of integrable motion and chaotic motion. Since

the wave packet expands more effectively during the chaotic motion, the data points with large \hbar for both A and B lie closer to the fitting curve for the chaotic motion.

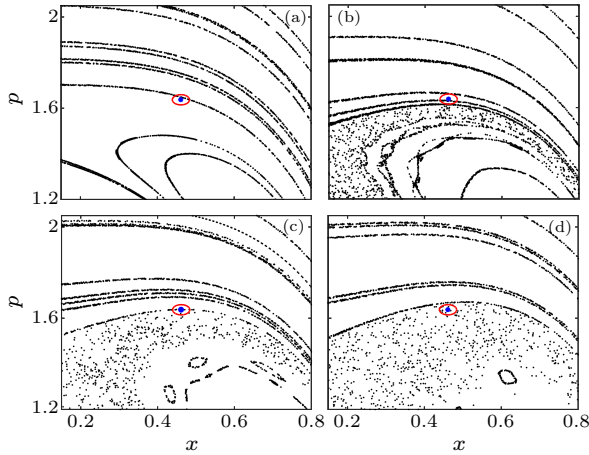


Fig. 6. As the driving strength A increases, the classical dynamics of the initial condition ($x_0 = 0.4614$, $p_0 = 1.637$) changes from integrable to chaotic. (a) $A = 0.10$, (b) $A = 0.28$, (c) $A = 0.36$ and (d) $A = 0.50$. The red circles indicate the size of wave packets with $\tilde{\hbar} = 0.001$.

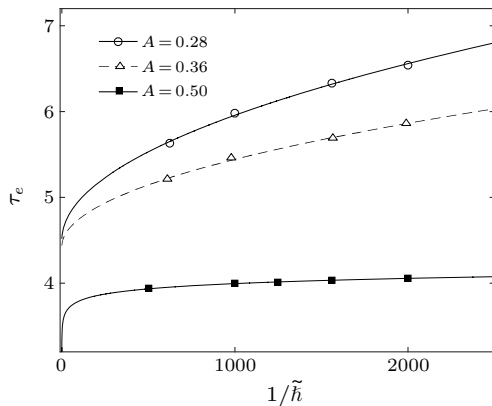


Fig. 7. Relationships between Ehrenfest time τ_e and $1/\tilde{\hbar}$ for the point shown in Fig. 6 ($x_0 = 0.4614$, $p_0 = 1.637$), with three different driven strengths $A = 0.28$, $A = 0.36$ and $A = 0.50$. Ehrenfest time for $A = 0.28$ is fitted by the function $\tau_e = 0.0460\tilde{\hbar}^{-1/2} + 4.50$, and Ehrenfest time of $A = 0.50$ is fitted by the function $\tau_e = 0.0879 \ln \tilde{\hbar}^{-1} + 3.39$. The dashed line for $A = 0.36$ indicates the trend of data.

We consider a situation shown in Fig. 6. In this case, the location of the initial wave packet, marked by the red circle in the figure, in the phase space does not change but the driving strength A is changing. When A is small, the classical dynamics of the anharmonic oscillator is mostly integrable and the initial wave packet lies entirely in the integrable region of the phase space. As A increases, the system gradually becomes more chaotic as evident from its Poincaré section. As a result, the initial wave packet begins to have some overlap with the chaotic region. When A is large enough, the initial wave packet lies completely in the chaotic region. Figure 7 shows the gradual evolu-

tion of Ehrenfest time during this process. When the wave packet is mainly located in the integrable region ($A = 0.28$), Ehrenfest time is large and is inversely proportional to the square root of \hbar , $\tau_e \propto \tilde{\hbar}^{-1/2}$. When the wave packet is located in the chaotic region ($A = 0.50$), Ehrenfest time becomes smaller and logarithmic, $\tau_e \propto \ln \tilde{\hbar}^{-1}$. For the intermediate process ($A = 0.36$), Ehrenfest time is between those of integrable motion and chaotic motion. As the motion of the wave packet changes from integrable to chaotic, Ehrenfest time becomes smaller. According to the above analysis, we can conclude that the dependence of Ehrenfest time on the Planck constant should change gradually with A .

In summary, we have studied the Ehrenfest time of an anharmonic oscillator, in particular, its dependence on the Planck constant at the transition from integrable motion to chaotic motion. We have found that at the transition the dependence is a mixture of integrable and chaotic motions. Although our study is carried out with a particular system, an anharmonic periodically driven oscillator, the same conclusion is expected to be drawn in other chaotic dynamical systems, as a result of typical structure of the phase space. Ehrenfest time of an initial well-localized wave packet depends not only on the Planck constant but also on its location when the system is not fully integrable or chaotic.

We thank Chao Yin for helpful discussion.

References

- [1] Ehrenfest P 1927 *Z. Phys.* **45** 455
- [2] Combesure M and Robert D 1997 *Asymptotic Anal.* **14** 377
- [3] Hagedorn G and Joye A 2000 *Ann. Henri Poincaré* **1** 837
- [4] Berry M V 1979 *J. Phys. A* **12** 625
- [5] Berman G and Zaslavsky G 1978 *Physica A* **91** 450
- [6] Zaslavsky G M 1981 *Phys. Rep.* **80** 157
- [7] Silvestrov P G and Beenakker C W J 2002 *Phys. Rev. E* **65** 035208
- [8] Grepel D R, Fishman S and Prange R E 1984 *Phys. Rev. Lett.* **53** 1212
- [9] Tian C, Kamenev A and Larkin A 2005 *Phys. Rev. B* **72** 045108
- [10] Fishman S, Grepel D R and Prange R E 1987 *Phys. Rev. A* **36** 289
- [11] Lai Y C, Ott E and Grebogi C 1993 *Phys. Lett. A* **173** 148
- [12] Berman G, Iomin A and Zaslavsky G 1981 *Physica D* **4** 113
- [13] Berman G P, Bulgakov E N and Holm D D 1994 *Crossover-Time in Quantum Boson and Spin Systems in Lecture Notes in Physics Monographs* (Berlin: Springer)
- [14] Zhao Y and Wu B 2019 *Sci. Chin. Phys. Mech. & Astron.* **62** 997011
- [15] Habib S, Shizume K and Zurek W H 1998 *Phys. Rev. Lett.* **80** 4361
- [16] Arnold V I 1978 *Mathematical Methods of Classical Mechanics* (Berlin: Springer) vol 60
- [17] Robinett R W 2004 *Phys. Rep.* **392** 1
- [18] Bakman A, Veksler H and Fishman S 2017 *Phys. Lett. A* **381** 2298
- [19] Veksler H and Fishman S 2015 *New J. Phys.* **17** 053030
- [20] Izrailev F M 1990 *Phys. Rep.* **196** 299

Chinese Physics Letters

Volume 38

Number 3

March 2021

GENERAL

- 030301 **Two-Dimensional Quantum Walk with Non-Hermitian Skin Effects**
Tianyu Li, Yong-Sheng Zhang, and Wei Yi
- 030302 **Effects of Quantum Noise on Quantum Approximate Optimization Algorithm**
Cheng Xue, Zhao-Yun Chen, Yu-Chun Wu, and Guo-Ping Guo
- 030303 **Experimental Protection of the Spin Coherence of a Molecular Qubit Exceeding a Millisecond** **Express Letter**
Yingqiu Dai, Yue Fu, Zhifu Shi, Xi Qin, Shiwei Mu, Yang Wu, Ji-Hu Su, Yi-Fei Deng, Lei Qin, Yuan-Qi Zhai, Yan-Zhen Zheng, Xing Rong, and Jiangfeng Du
- 030304 **Quantum Algorithm for Approximating Maximum Independent Sets** **Express Letter**
Hongye Yu, Frank Wilczek, and Biao Wu
- 030501 **Advection and Thermal Diode**
Ying Li and Jiaxin Li
- 030502 **Ehrenfest Time at the Transition from Integrable Motion to Chaotic Motion**
Chuan Zhao and Biao Wu

NUCLEAR PHYSICS

- 032301 **Quantum Anti-Zeno Effect in Nuclear β Decay**
Ming Ji and Chang Xu

FUNDAMENTAL AREAS OF PHENOMENOLOGY (INCLUDING APPLICATIONS)

- 034101 **Effective Interaction Force between an Electric Charge and a Magnetic Dipole and Locality (or Nonlocality) in Quantum Effects of the Aharonov–Bohm Type**
Gianfranco Spavieri, George T. Gillies, Miguel Rodriguez, and Maribel Perez
- 034201 **Ultra-Broadband Infrared Metamaterial Absorber for Passive Radiative Cooling**
Yan-Ning Liu, Xiao-Long Weng, Peng Zhang, Wen-Xin Li, Yu Gong, Li Zhang, Tian-Cheng Han, Pei-Heng Zhou, and Long-Jiang Deng

PHYSICS OF GASES, PLASMAS, AND ELECTRIC DISCHARGES

- 035201 **Nonlinear Coupling of Reversed Shear Alfvén Eigenmode and Toroidal Alfvén Eigenmode during Current Ramp**
Shizhao Wei, Yahui Wang, Peiwan Shi, Wei Chen, Ningfei Chen, and Zhiyong Qiu
- 035202 **Energetic Particle Physics on the HL-2A Tokamak: A Review** **Review**
Pei-Wan Shi, Wei Chen, and Xu-Ru Duan

CONDENSED MATTER: STRUCTURE, MECHANICAL AND THERMAL PROPERTIES

- 036201 **Novel Superconducting Electrides in Ca–S System under High Pressures**
Yun-Xian Liu, Chao Wang, Shuai Han, Xin Chen, Hai-Rui Sun, and Xiao-Bing Liu
- 036301 **Quantum Transport across Amorphous-Crystalline Interfaces in Tunnel Oxide Passivated Contact Solar Cells: Direct versus Defect-Assisted Tunneling**
Feng Li, Weiyuan Duan, Manuel Pomaska, Malte Köhler, Kaining Ding, Yong Pu, Urs Aeberhard, and Uwe Rau

CONDENSED MATTER: ELECTRONIC STRUCTURE, ELECTRICAL, MAGNETIC, AND OPTICAL PROPERTIES

- 037401 **Superconductivity and Charge Density Wave in Iodine-Doped CuIr_2Te_4**
Mebrouka Boubeche, Jia Yu, Li Chushan, Wang Huichao, Lingyong Zeng, Yiyi He, Xiaopeng Wang, Wanzhen Su, Meng Wang, Dao-Xin Yao, Zhijun Wang, and Huixia Luo

- 037402 Gate Tunable Supercurrent in Josephson Junctions Based on Bi₂Te₃ Topological Insulator Thin Films**
Wei-Xiong Wu, Yang Feng, Yun-He Bai, Yu-Ying Jiang, Zong-Wei Gao, Yuan-Zhao Li, Jian-Li Luan, Heng-An Zhou, Wan-Jun Jiang, Xiao Feng, Jin-Song Zhang, Hao Zhang, Ke He, Xu-Cun Ma, Qi-Kun Xue, and Ya-Yu Wang
- 037403 Superconductivity and Normal-State Properties of Kagome Metal RbV₃Sb₅ Single Crystals**
Qiangwei Yin, Zhijun Tu, Chunsheng Gong, Yang Fu, Shaohua Yan, and Hechang Lei
- 037501 Exotic Dielectric Behaviors Induced by Pseudo-Spin Texture in Magnetic Twisted Bilayer **Express Letter****
Yu-Hao Shen, Wen-Yi Tong, He Hu, Jun-Ding Zheng, and Chun-Gang Duan
- 037701 Observation of Ferroelastic and Ferroelectric Domains in AgNbO₃ Single Crystal**
Wei Zhao, Zhengqian Fu, Jianming Deng, Song Li, Yifeng Han, Man-Rong Li, Xueyun Wang, and Jiawang Hong

CROSS-DISCIPLINARY PHYSICS AND RELATED AREAS OF SCIENCE AND TECHNOLOGY

- 038101 Phase Stability and Hydroxyl Vibration of Brucite Mg(OH)₂ at High Pressure and High Temperature**
Wei-Bin Gui, Chao-Shuai Zhao, and Jin Liu
- 038102 Au Films Composed of Nanoparticles Fabricated on Liquid Surfaces for SERS**
Xunheng Ye, Jiawei Shen, Xiangming Tao, Gaoxiang Ye, and Bo Yang
- 038701 A Linear Frequency Principle Model to Understand the Absence of Overfitting in Neural Networks**
Yaoyu Zhang, Tao Luo, Zheng Ma, and Zhi-Qin John Xu

GEOPHYSICS, ASTRONOMY, AND ASTROPHYSICS

- 039801 Klein–Nishina Effect and the Cosmic Ray Electron Spectrum **Express Letter****
Kun Fang, Xiao-Jun Bi, Su-Jie Lin, and Qiang Yuan

ERRATA AND OTHER CORRECTIONS

- 039901 Erratum: A Ubiquitous Thermal Conductivity Formula for Liquids, Polymer Glass, and Amorphous Solids [Chin. Phys. Lett. 37 (2020) 104401]**
Qing Xi, Jinxin Zhong, Jixiong He, Xiangfan Xu, Tsuneyoshi Nakayama, Yuanyuan Wang, Jun Liu, Jun Zhou, and Baowen Li

JUST FOR AUTHORS
— CHINESE PHYSICS LETTERS